Surface production of negative deuterium ions from plasma-exposed boron doped diamond and graphite: work function measurements using photoemission yield spectroscopy

Ryan Magee, Brandan Maurice, Joey Demiane, Jean-Marc Layet, Timo Gans, James P Dedrick, Gilles Cartry

Plasma Sources Science and Technology

PAPER • **OPEN ACCESS**

Surface production of negative deuterium ions from plasma-exposed boron doped diamond and graphite: work function measurements using photoemission yield spectroscopy

To cite this article: Ryan Magee *et al* 2023 *Plasma Sources Sci. Technol.* **32** 075021

OPEN ACCESS
IOP Publishing
Plasma Sources Science and Technology
Plasma Sources Sci. Technol. **32** (2023) 075021 (10pp)
https://doi.org/10.1088/1361-6595/ace6d1

Surface production of negative deuterium ions from plasma-exposed boron doped diamond and graphite: work function measurements using photoemission yield spectroscopy

Ryan Magee[1,*], Brandan Maurice[2], Joey Demiane[2], Jean-Marc layet[2], Timo Gans[3], James P Dedrick[1] and Gilles Cartry[2]

[1] York Plasma Institute, Department of Physics, University of York, Heslington, York YO10 5DD, United Kingdom
[2] Aix-Marseille Université/CNRS, PIIM, UMR 6633, Centre de St Jérôme, Case 241, 13397 Marseille Cedex 20, France
[3] School of Physical Sciences, National Centre for Plasma Science and Technology, Faculty of Science and Health, Dublin City University, Dublin, Ireland

E-mail: ryan.magee@york.ac.uk

Received 15 May 2023, revised 5 July 2023
Accepted for publication 12 July 2023
Published 3 August 2023

Abstract

Negative-ion sources are of considerable interest for applications such as materials processing and neutral beam injection for magnetic confinement fusion. The efficient production of negative ions in these sources often relies on surface production. Work function measurements are critical to enable a detailed understanding of the mechanisms that underpin this. In this study we used a combination of photoemission yield spectroscopy and the Fowler method to determine the work functions of boron doped diamond (BDD) and highly oriented pyrolytic graphite (HOPG) directly after exposure to a low-pressure inductively coupled deuterium plasma (150 W, 2 Pa). A magnetised retarding field energy analyser is used to measure the negative ion current from the samples. During plasma exposure, samples are biased at −130 V or −60 V and their temperature is varied between 50 °C and 750 °C. The results show that the increasing work function of the plasma exposed HOPG occurs over the same sample temperature range as the decreasing negative-ion current. In contrast, the work function of BDD does not show a clear relationship with negative-ion current, suggesting that different mechanisms influence the negative-ion production of metal-like HOPG and dielectric-like BDD. The necessity for an additional fitting parameter for the Fowler fits to BDD suggests that its electronic properties are changing under plasma exposure, unlike HOPG. For both materials, the maximum photocurrent measured from the samples displays a strong similarity with negative-ion current, suggesting

* Author to whom any correspondence should be addressed.

they are driven by a common mechanism. The *in-situ* measurement of the work function using non-invasive techniques is of interest for the development of negative ion sources.

Keywords: deuterium plasma, negative ions, surface production

(Some figures may appear in colour only in the online journal)

1. Introduction

Negative ions are of significant interest due to their influence on the plasma physics in semiconductor processing [1, 2], ion thrusters [3–5], particle acceleration [6–9], and neutral beam injection (NBI) systems for tokamaks [10–13].

Negative ions play a particularly important role in hydrogen plasmas and are the primary species of interest for NBI systems in ITER [14]. For these systems, where a large current of negative-ions is required, low work function metals like caesium are put in contact with the hydrogen plasma inside the ion source to promote negative-ion surface production [15, 16]. The use of caesium comes with significant engineering challenges [11, 15, 17], and therefore alternative materials are being investigated. Examples of different materials being studied include highly oriented pyrolytic graphite (HOPG) [18], electrides such as C12A7 [19], and dielectrics, namely diamond [20–22]. While the occupied states in the valence band are at a lower level in dielectrics than that of conductors, the added difficulty of capturing electrons may be countered by the reduction in electron loss back to the material due to the presence of the band gap [20].

Diamond is of significant interest because its physical and electronic properties can be easily manipulated through the manufacturing process and doping [20, 23]. In previous work, the negative-ion yield from boron doped microcrystaline diamond (BDD) and HOPG under exposure to deuterium plasma have been compared [20, 22, 24]. They have been shown to exhibit strong and very different surface temperature dependencies, with the yield from HOPG continuously decreasing when the surface temperature increases while the yield from BDD passes through a maximum at about 400 °C–500 °C.

The physical mechanisms that underpin the production of negative ions from HOPG and BDD are complex. Under plasma exposure, a top surface of amorphous hydrogenated carbon with a certain sp^2/sp^3 hybridization ratio is created on HOPG (sp^2) and BDD (sp^3) [24]. Negative ions are produced from this top layer through the backscattering of incoming positive ions or the sputtering of adsorbed hydrogen atoms accompanied by the capture of an electron from the surface [25]. The negative-ion yield Y_{NI} is therefore proportional to the product of the surface ionization probability P_{iz} and the sum of the yields from backscattering and sputtering [26] as shown in equation (1):

$$Y_{NI} = P_{iz}(Y_B + Y_S) \tag{1}$$

where Y_B and Y_S are the yields from backscattering and sputtering, respectively.

While the backscattering yield has not been observed to vary strongly with the temperature of the sample [27], the sputtering yield can change significantly due to variations in the hydrogen sub-surface content. Previous modelling of the negative-ion emission has suggested that for BDD the content of sub-surface hydrogen increased only slightly (from 30% to 35%) as the temperature of the sample changed between room temperature and 500 °C. As distinct from this, for HOPG, the hydrogen sub-surface content decreased continuously by a relatively large amount (30% to zero) over the same temperature range [20]. It is interesting to note that the observed variation in the hydrogen sub-surface content led to only a factor two change in the negative-ion yield, which is not sufficient to fully account for the variations observed in independent experiments [24]. It is therefore reasonable to suggest that the ionisation probability P_{iz}, which changes with sample temperature due to variations in the surface state [24] and sub-surface hydrogen content, could be significant.

Previous Raman spectroscopy measurements have shown that the sp^2/sp^3 hybridization ratio of the layer, upon which negative ions are produced, is indeed changing with the temperature of the sample. For increasing sample temperatures, sp^2 and sp^3 defects decrease for BDD and HOPG, respectively. In other words, the material recovers towards a pristine state as the temperature of the sample is increased [24].

As described above, for BDD the negative-ion yield exhibits a peak at 400 °C–500 °C, which can be attributed to an optimal value of P_{iz} due to the sp^2/sp^3 ratio, and possibly to the recovery of some of the hydrogenated diamond properties such as the negative electron affinity [20, 22, 24]. For sample temperatures above 400 °C–500 °C, the decrease in the negative ion yield was attributed to a decrease in the ionisation probability caused by a combination of insufficient sp^2/sp^3 ratio, decreasing hydrogen content in the sub-surface, and possibly the loss of negative electron affinity. In the distinct case of HOPG, the authors attributed the continuously decreasing negative ion yield to an overly large sp^2/sp^3 ratio, which caused a decrease in the sputtering yield and ionisation probability.

In order to confirm the link between the surface state of the material and negative ion yield, which is mediated by changes in the ionisation probability with surface temperature, it is of significant interest to measure the ionisation energy *in situ*. This is known as work function for a metal, and ionisation energy for a dielectric, for simplicity, we use the term work function for both BDD and HOPG in this paper [28].

Photoemission yield spectroscopy (PYS) is an established technique [29], which can be combined with the Fowler method [30] to determine the work function of surfaces [31–36]. For example, it has been employed to show that the

work function of caesium-coated molybdenum changes significantly with plasma exposure [37–39]. The similar technique of ultra-violet photoemission spectroscopy has previously been applied to measure the work function of annealed BDD [40, 41].

In this study, we employ PYS to investigate changes in the the work function and negative ion yield with respect to the temperature of BDD and HOPG samples. HOPG is used as a reference of a conducting carbon material that has undergone extensive previous research [18, 25, 42].

The experimental methods are described in section 2: plasma source and sample holder in section 2.1, HOPG and BDD samples in section 2.2, optical setup in section 2.3, measurement procedure in section 2.4, and analysis method in section 2.5. Results of negative-ion current and PYS measurements on HOPG and BDD are presented in sections 3.1 and 3.2, respectively.

2. Method

2.1. Plasma source

The experimental setup is shown in figure 1.

The plasma source, which is shown in figure 1(a) and described in detail in [43], consists of an inductively coupled plasma (ICP) produced by using an RF generator (Huttinger PFG 1600, 13.56 MHz, 150 W) coupled to a three-turn planar coil via a matching network (Huttinger PFM 3000 A matchbox). Deuterium gas is fed into the chamber at 7.4 sccm through a mass flow controller (Brooks 5850 TR) where it is held at 2 Pa by a scroll pump (Edwards nXDS10i), a turbo molecular pump (Alcatel ATP 400) and an adjustable valve. Following its production in the source region, the plasma expands through a grounded mesh into the diffusion chamber.

Inside the diffusion chamber, samples are held in place by a molybdenum clamp on a four-axis sample holder as shown in figure 1(b) and described in detail in [43]. The sample is biased at −60 V and −130 V by a DC voltage source (ES CN7) for 'low energy' and 'high energy' ion bombardment, with corresponding positive ion currents incident onto the sample of 22 μA and 26 μA (2.7 and 3.2 $\times 10^{18}$ ions m^{-2} s^{-1}), respectively. The temperature of the sample T_s is regulated within 50 °C–750 °C using a tungsten filament and a thermocouple placed in the sample holder.

2.2. HOPG and BDD samples

New samples of HOPG and BDD were introduced into the chamber for each set of measurements. Each HOPG sample was freshly cleaved just before loading into the chamber. HOPG samples (surface area 12×12 mm^2 and thickness 2 mm) were of ZYB type and had density and electrical resistivity of 2.265 g cm^{-3} and $3.5 \times 10^{-5}\,\Omega$ cm, respectively [24]. Micro-crystalline BDD samples were purchased from NeoCoat. The deposited BDD layer had a thickness of 3 μm and a charge carrier density of approximately 2.0×10^{20} cm^{-3}.

2.3. Optical setup for PYS

PYS measurements were undertaken by illuminating the sample with monochromatic light scanned over the range 200 nm $< \lambda <$ 450 nm of the incident wavelength λ. The light source (300 W xenon lamp) is integrated with a monochromator (Zolix omni-λ 300i). The monochromatic light ($\pm$5 nm) is fed through an optical fibre bundle to produce a circular beam that is passed through a chopper set at 35 Hz to modulate the output. As shown in figure 1(c), the modulated beam is focused through the viewing port via a cone and onto the sample by a lens doublet. The tip of the cone is placed 1 mm away from the sample. Consequently the reflected light primarily travels back through the cone and light reflected off other surfaces of the chamber, which could influence the current measured on the sample, is minimised. The cone is biased at 7.5 V to collect emitted electrons and prevent charge build up on the surface. The sample current is converted into a voltage by a Keithley 6482 ammeter connected to the sample, and then fed into a Zurich Instrument MFLI lockin amplifier to detect its component at the light modulation frequency (35 Hz).

2.4. Procedure for the measurement of the samples

The measurement procedure was as follows:

- Plasma was ignited in the chamber and left for 30 min to condition the walls (exposure conditions: ICP using D_2 gas at 150 W and 2 Pa with a plasma potential of 7 V.)
- The samples were heated to temperature T_s, and simultaneously biased at V_D for 5 min. A settling time of 5 min was added to this to ensure steady-state conditions.
- The gas supply to the source region, and the RF generator that powers the ICP coil, were switched off to turn off the plasma and limit external influences on sample current.
- The sample bias voltage V_D was removed and the photocurrent measurement system connected via switches 1 and 2, respectively, in figure 1(b). The cone bias was also switched on.
- The heating filament, attached to the sample to control its temperature to *Ts* as shown in figure 1(b) was switched off. Approximately 45 s passes between switching the plasma off and starting the measurement of the photocurrent.
- The 35 Hz modulated photocurrent was measured with respect to wavelength of the incident light for 200 nm $< \lambda <$ 450 nm and used to determine the energy at which electrons are released from the material. The duration of the measurement is approximately 1 min.

More details are given on the PYS measurements in section 2.5.

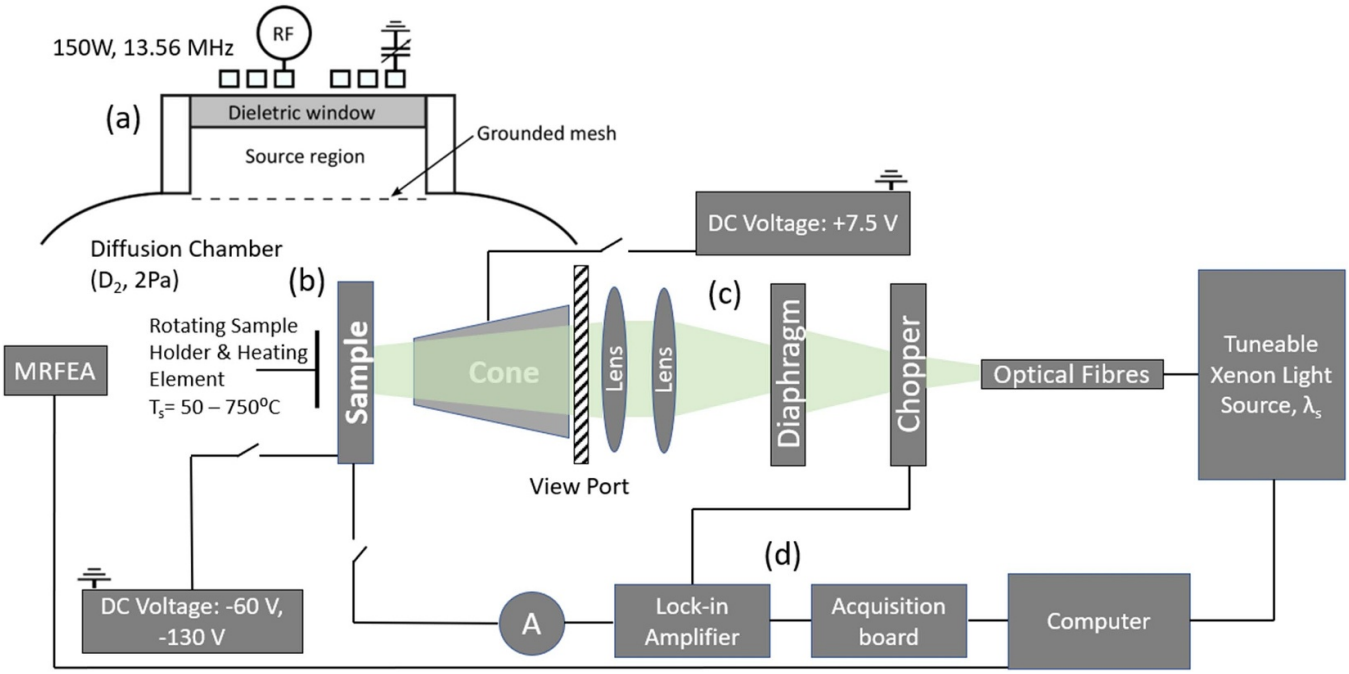

Figure 1. Set up of the experiment. (a) ICP plasma source, (b) diffusion chamber containing mounted sample with temperature control, (c) optical setup for photoemission yield spectroscopy including UV view port, and (d) photocurrent measurement system with synchronised chopper and lock-in amplifier. The figure is not drawn to scale.

2.5. Determining the work function using Fowler fits to the photocurrent data

Figure 2 shows the results of the photocurrent measurements.

For each material, shown in figure 2, the background of the measurement was defined as the average sample current measured over the range of photon energies 2.75 eV (451 nm) $<$ hν $<$ 3.2 eV (387 nm). As the measured background was seen to change between measurements, the raw data was shifted so that each data set had a common background. In figure 2, the background has been removed from each curve for clarity. Following background removal the photocurrent data was corrected by the spectral response of the diagnostic system, taking into account the lamp, optical impedance of the fibre, collimating lenses, and the UV view port as shown in figure 1. Each data set was also divided by the square of the sample temperature for fitting purposes as used in [39]. We refer to this measurement as the corrected photocurrent $I_{\mathrm{ph,c}}$.

$$I_{\mathrm{ph,c}} = \frac{I_{\mathrm{ph}}}{F(h\nu)T_s^2} \tag{2}$$

where $F(h\nu)$ is the wavelength dependant relative intensity of the light incident on the sample.

As an additional metric, the spectrally corrected photocurrent, excluding temperature correction, is determined at a photon energy of 5.4 eV because this is where it is observed to reach a maximum value for each value of T_s (not shown but can be inferred from figure 2). We refer to this as the maximum photocurrent $I_{\mathrm{ph,max}}$, which is used to make a correlation between the photoelectron flux and the negative ion flux, both of which depend on the work function.

The dashed lines in figure 2 are Fowler fits of the corrected photocurrent. The Fowler theory describes the photoemission yield Y_{ph} of metals with respect to the wavelength of incident light close to the photoemission threshold [30, 39] as follows:

$$Y_{\mathrm{ph}} = A\left(\frac{\pi^2}{6} + \frac{1}{2}\mu^2 - \mathrm{e}^{-\mu} + \frac{\mathrm{e}^{-2\mu}}{2^2} - \frac{\mathrm{e}^{-3\mu}}{3^2} + \cdots\right) \tag{3}$$

with

$$\mu = \frac{h\nu - \chi}{k_{\mathrm{B}}T_s} \quad , \quad h\nu \geqslant \chi \tag{4}$$

where k_{B} is the Boltzmann constant and χ is the work function. The factor A is made of physical constants and proportionality factors.

Fowler fits are made to the corrected photocurrent data using equation (5). This is a truncated version of equation (3), where we eliminate the higher order exponential terms that have very little influence on the fitting:

$$I_{\mathrm{ph,c}} = A\left(\frac{\pi^2}{6} + \frac{1}{2}\mu^2 - \mathrm{e}^{-\mu}\right). \tag{5}$$

Fowler fits according to equation (5) are made using orthogonal distance regression and used to estimate the work function χ of the plasma exposed samples as a function of their temperature T_s. Within the framework of the Fowler theory, the parameter A is a constant. It was fitted for the 200 °C case for HOPG and kept at this value for the other HOPG data. Applying this method to BDD produced poor fitting due to

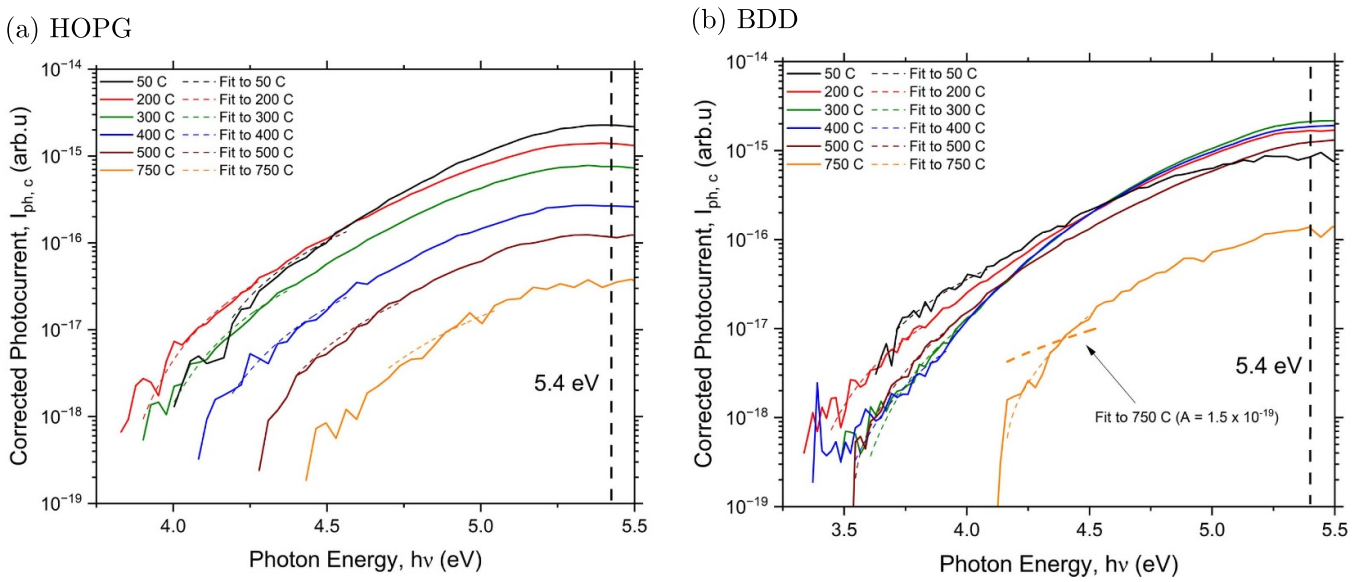

Figure 2. Corrected photocurrent with respect to incident photon energy and sample temperature as measured for (a) HOPG and (b) BDD samples, both at −130 V bias. The photocurrent is measured after plasma exposure. Details of the fitting parameters are given in table 1.

Table 1. Values of parameter A for the Fowler fitting for BDD and HOPG. The value of A is fitted for BDD and fixed for HOPG.

	Fitting parameter A ($\times 10^{-19}$)		
Temperature, T_s (°C)	HOPG −130 V	BDD −130 V	BDD −60 V
50	7.2	1.6	0.9
200	7.2	1.5	7.3
300	7.2	3.1	22.9
400	7.2	2	21.6
500	7.2	6.1	35
600	7.2	9.6	23.8
750	7.2	18.3	22.2

varying photocurrent gradients for distinct sample temperatures as observed in the clearly inaccurate fit for the data corresponding to $T_s = 750\,°C$, figure 2(b), with $A = 1.5 \times 10^{-19}$ (the value of A fitted for $T_s = 200\,°C$). Therefore, A was used as an additional fitting parameter for the BDD samples. The values for parameter A are shown in table 1.

Table 1 shows that the fitted A parameter for BDD increases significantly in both the −130 V and −60 V cases. The necessity for fitting A for BDD suggests that it is not behaving as a metal, i.e. its electronic properties are changing. In contrast, the use of a fixed A value for HOPG suggests it is behaving as a metal at all temperatures. This is discussed further in sections 3.1 and 3.2. BDD measurements were taken with bias voltages of −60 V and −130 V, HOPG was only taken at −130 V due to previous work from [26] figure 9 indicating that the −60 V and −130 V cases are very similar for this material.

The lower-photon-energy limit for the Fowler fitting was taken as the lowest photocurrent that is larger than the background noise level. The upper-photon-energy limit was set to be 0.4 eV above the lower photon-energy-limit. This is used as a conservative estimate of where the photocurrent is significantly larger than the noise in the background current. A photon-energy range of 0.4 eV was selected as the Fowler fitting is only valid near the threshold [30, 39]. Error bars for the work function χ in all HOPG and BDD cases are calculated as shown in equation (6):

$$\Delta\chi = \frac{hc\Delta\lambda}{e\lambda^2} \tag{6}$$

This is due to the ±5 nm resolution of the monochromator as described in section 2.3.

2.6. Magnetised retarding field energy analyser (MRFEA) for measurement of negative-ion current

An MRFEA [44, 45], shown in figure 1, was used to measure the negative-ion current β from the BDD and HOPG samples. It should be noted that the negative-ion current is proportional to negative-ion yield in the case of a constant incident positive ion flux, i.e. a constant sample bias, which is the case in our system for a given DC bias voltage applied to the sample.

The MRFEA incorporates a single collector grid, which is located downstream of a magnetic barrier. This barrier prevents the passage of electrons produced in the bulk plasma and secondary electrons from reaching the detector, as described in [44, 45]. The voltage at the collector grid is scanned (Kiethley 2450 SourceMeter) to enable the measurement of the energy-resolved number distributions of distinct populations for positive ions, negative ions, and electrons.

As with the PYS measurements, the sample bias voltage was applied in parallel with the heating of the samples. Approximately 1 min was allowed to elapse prior to each measurement to enable stabilisation.

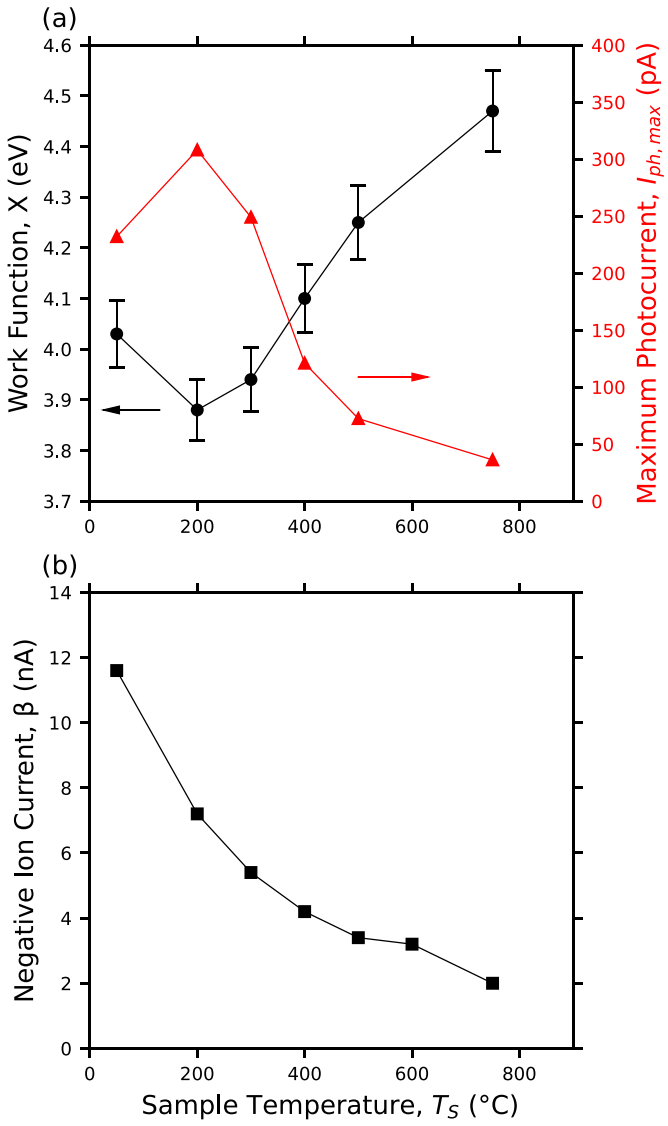

Figure 3. (a) Work function and maximum photocurrent with respect to sample temperature after exposure to a 2 Pa, 150 W deuterium plasma. (b) Negative-ion current (measured with the MRFEA) with respect to sample temperature. HOPG sample biased at −130 V.

3. Results

3.1. Work function, photocurrent, and negative-ion current from HOPG

Figure 3 shows the work function, maximum photocurrent $I_{\mathrm{ph,max}}$, and negative-ion current β with respect to temperature of an HOPG sample after exposure to deuterium plasma with a sample bias of −130 V. The changes in negative-ion current with respect to the sample temperature shown in figures 3–5, are consistent with previous measurements for which a distinct diagnostic approach was used [20, 22, 24, 46].

In figure 3(a) the work function is shown to be just over 4.0 eV at 50 °C, then drops to 3.9 eV after which it consistently increases with respect to sample temperature up to 4.5 eV for temperatures 200 °C $< T_s <$ 750 °C. The work function of pristine graphite is 4.6 eV [47]. Therefore this result is in agreement with the Raman spectroscopy measurements in [20, 24], which showed that with low temperature hydrogen plasma exposure a hydrogenated amorphous carbon layer forms and as temperature is increased up to 800 °C, the pristine graphite surface is close to being fully restored through annealing of defects and outgassing of hydrogen. The accurate Fowler fitting with a constant value of A for all temperatures shows that the HOPG surface continues to behave as a metal after plasma exposure for sample temperatures within the range 50 °C–750 °C.

Displaying a very similar but inverted trend to that of the work function, at 50 °C the maximum photocurrent $I_{\mathrm{ph,max}}$ is around 230 pA before increasing to 300 pA at 200 °C and subsequently decreasing to 250 pA, 120 pA, 70 pA, and 35 pA for temperatures 300 °C $< T_s <$ 750 °C, respectively. This is expected for a metal-like surface because the increasing work function means electrons are harder to release and therefore a lower total current should be measured, as consistent with the decreasing $I_{\mathrm{ph,max}}$ over the same T_s range.

The negative-ion current, shown in figure 3(b), continuously decreases for increasing values of T_s from approximately 12 nA at 50 °C to 2 nA at 750 °C. In the region between 200 °C and 750 °C, this trend is consistent with the work function measurements in figure 3(a) showing that at lower temperatures, electrons are more easily released from the material and therefore electron capture from the incoming deuterium atoms and positive ions is more likely to take place, hence leading to larger negative-ion current. This is consistent with the known negative-ion production mechanisms for metallic materials for which the yield is observed to be strongly correlated with the work function [48]. Both the work function and the negative ion current decrease for increasing sample temperature between 50 °C and 200 °C. It is reasonable to suggest that this tendency, opposite to that observed between 200 °C and 750 °C, is caused by the decrease of the sub-surface hydrogen density which contributes to negative-ion production through the sputtering term, as seen in equation (1).

3.2. Work function, photocurrent, and negative-ion current of BDD

Figure 4 shows the work function, maximum photocurrent $I_{\mathrm{ph,max}}$, and negative-ion current with respect to sample temperature at −130 V bias for a BDD sample.

The work function in figure 4(a) is observed to fluctuate between 3.3 eV and 3.6 eV for sample temperatures 50 °C $< T_s <$ 500 °C before increasing to 3.8 eV and 4.2 eV at 600 °C and 750 °C, respectively. The negative-ion current in figure 4(b) starts at approximately 20 nA at 150 °C, peaks at 30 nA at 400 °C, and then drops down to 15 nA at 700 °C. The small fluctuations in work function between 50 °C $< T_s <$ 500 °C are seen over roughly the same temperature range that negative-ion current clearly rises (between 150 °C $< T_s <$ 400 °C). The rise of negative-ion current is thus not correlated with a decrease in work function. This is in agreement with the

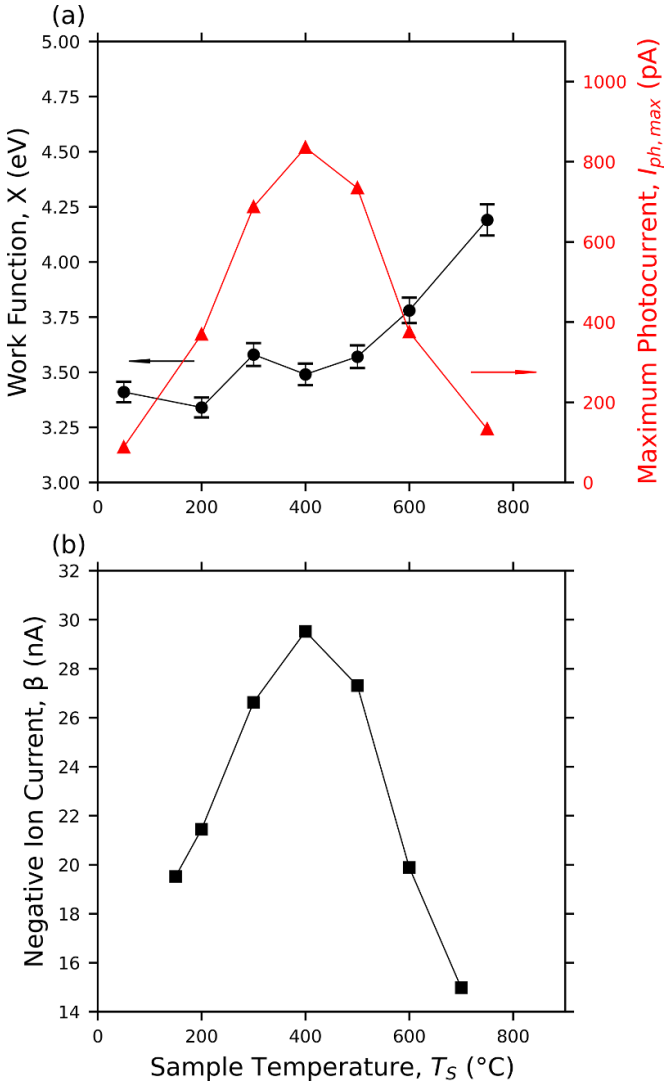

Figure 4. (a) Work function and maximum photocurrent with respect to sample temperature after exposure to a 2 Pa, 150 W deuterium plasma. (b) Negative-ion current (measured with the MRFEA) with respect to sample temperature. BDD sample biased at −130 V.

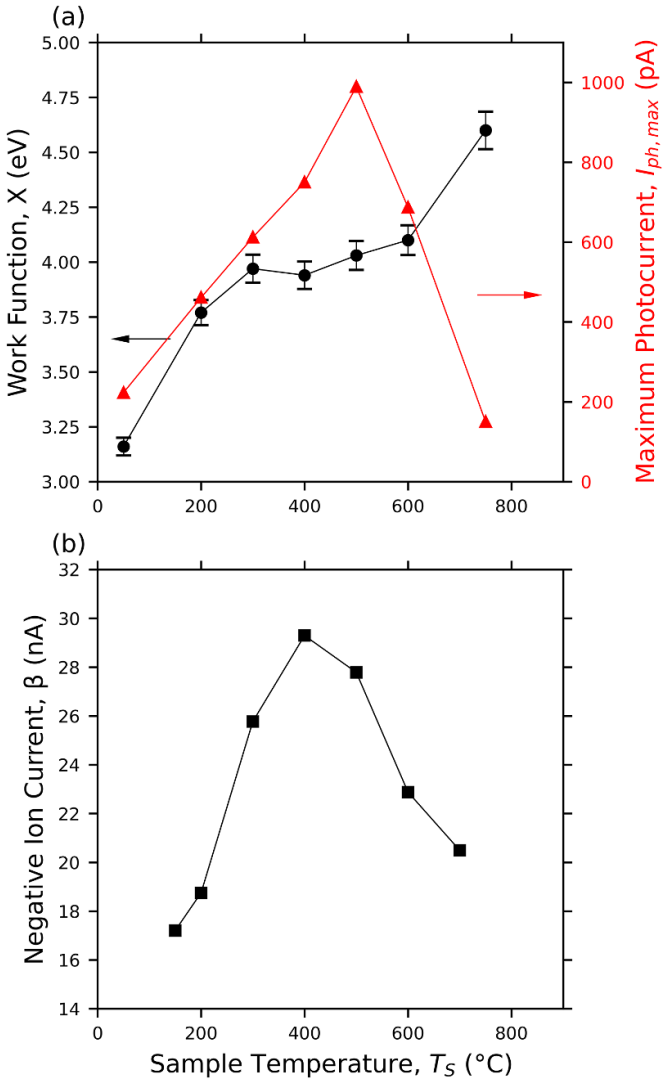

Figure 5. (a) Work function and maximum photocurrent with respect to sample temperature after exposure to a 2 Pa, 150 W deuterium plasma. (b) Negative-ion current (measured with the MRFEA) with respect to sample temperature. BDD sample biased at −60 V.

discussion of [49] where it is explained that the work function (or ionisation energy) is not the sole material property contributing to negative-ion yield for a dielectric-like material, and that the band gap in particular plays a strong role by limiting negative-ion destruction by electron loss back to the material.

The maximum photocurrent $I_{\mathrm{ph,max}}$ in figure 4(a) starts at around 90 pA at 50 °C and rises to a peak of 840 pA at 400 °C before falling back down to 130 pA at 750 °C. Interestingly, the initial increase in $I_{\mathrm{ph,max}}$ up to 400 °C displays similar behaviour to the negative-ion current over the same T_s range while the work function is seen to fluctuate around 3.5 eV, which suggests that a common mechanism underpins the electron photoemission and negative-ion production for BDD. The production of a photocurrent is a three-step process of optical absorption, transport of the electron through the bulk material to the surface, and escape from the surface to vacuum [50]. The similar trends between $I_{\mathrm{ph,max}}$ and negative-ion current, shown in figures 4(a) and (b), respectively, suggests that it is not the optical absorption that is influenced by the change in sample temperature. However, as described in [50], the presence of a band gap in a material can increase the photo-excited electron mean free path, hence increasing the escape probability and consequently the measured photocurrent. Therefore, changes in the plasma exposed diamond's electronic structure and the appearance of a band gap could explain the increase of the photoemission yield. In a similar way, negative-ion production from insulator-like materials depends not only on their work function, but also the presence of a band gap. This effectively decreases the probability that electrons can detach from the negative ion and return to the surface [49, 51–54]. Therefore, the reappearance of (or change in) the band gap as the temperature of the sample is increased is consistent with a similarity in the photocurrent

and negative-ion current, and the progressive reconstruction of an sp^3 diamond surface as previously observed via Raman spectroscopy in [24].

Figure 5 shows the work function, maximum photocurrent $I_{ph,max}$, and negative-ion current β with respect to BDD sample temperature at −60 V sample bias.

As in the −130 V case, shown in figure 4, the results for −60 V in figure 5 shows that $I_{ph,max}$ has a similar trend to negative-ion current at −60 V. $I_{ph,max}$ in figure 5(a) rises to 990 pA at 500 °C from 220 pA at 50 °C and recedes back down to 150 pA at 750 °C. The negative-ion current in figure 5(b) starts at 17 nA and shows a similar peak of approximately 30 nA but at 400 °C, and drops to 21 nA at 700 °C.

As for the measurement of BDD at −130 V, shown in figure 4, the work function in figure 5(a) displays no clear relationship with negative-ion current shown in figure 5(b). It starts just below 3.2 eV at 50 °C and increases to 3.75 eV, then stays around 3.9-4.0 eV between 300 °C and 500 °C before slightly increasing to 4.1 eV at 600 °C and jumping up to approximately 4.6 eV at 750 °C. Therefore, both the low and high energy ion bombardment cases are consistent with the discussion of [49] in showing that the work function is not the sole contributor to the negative-ion yield for dielectric-like materials.

Applying the same principles as in the −130 V case, the observed trend in the negative-ion current can be explained through the changing electronic properties in which a favourable surface state is created between 400 °C and 500 °C. Similarly, this surface state is also favorable for photoemission and we suggest this is due to a better transport of the electrons from the bulk to the surface as described in [50]. The subsequent decreases in $I_{ph,max}$, figures 4(a) and 5(a), and negative-ion current, figures 4(b) and 5(b), are correlated with the increasing work function.

The necessity for varying the A parameter when fitting the Fowler functions to both BDD cases, but not for HOPG, confirms results from a previous study in [20] that as the sample temperature of BDD is changed under exposure to hydrogen plasma, the electronic properties of the material are affected. As shown by the Raman spectroscopy measurements in [20], the graphite sp^2 phases (induced by bombardment from the plasma) gradually disappear with increasing temperature as the defects are annealed out until a near pristine diamond surface is returned to at around 800 °C.

4. Conclusion

We have investigated the effect of low pressure deuterium plasma exposure (150 W, 2 Pa) on the work functions of BDD and HOPG. Photocurrents were measured using PYS and a MRFEA was used to measure negative-ion current. The Fowler method was used to determine the work function from the photocurrent measurements and their analysis suggests the electronic properties of BDD change with plasma exposure, unlike HOPG. Similarities in trends between work function, maximum photocurrent, and negative-ion current at sample temperatures between 50 °C and 750 °C have been studied to examine the mechanisms of negative ion production. The work function and maximum photocurrent of HOPG display similar trends with the produced current of negative ions. The maximum photocurrent of BDD is also observed to follow the same qualitative trend as negative-ion current as the sample temperature is varied. However, the work function is seen to display a distinctly different trend. This highlights a clear difference in the behaviour of materials with metallic or dielectric-like electronic properties for negative-ion production.

Data availability statement

The data that support the findings of this study are openly available at the following URL/DOI: https://doi.org/10.15124/6960bcab-df9b-4467-a42d-81f9a576cbd7.

Acknowledgments

The authors would like to acknowledge the experimental support of Jean Bernard Faure and the rest of the PIIM group. This work has been carried out within the framework of the French Federation for Magnetic Fusion Studies (FR-FCM). The views and opinions expressed herein do not necessarily reflect those of the European Commission. The project that gave rise to this publication received funding from the Initiative of Excellence of Aix-Marseille University—A*Midex, Investissements d'Avenir Program AMX-19-IET-013. This project has also been supported by the Région Sud PACA through the Appel à Projets Recherche 2021—Volet exploratoire—Project SARDINE. The financial support of the EPSRC Centre for Doctoral Training in fusion energy is gratefully acknowledged under Financial Code EP/S022430/1.

ORCID iDs

Ryan Magee https://orcid.org/0000-0003-4153-5346
Joey Demiane https://orcid.org/0009-0001-5012-5771
Timo Gans https://orcid.org/0000-0003-1362-8000
James P Dedrick https://orcid.org/0000-0003-4353-104X
Gilles Cartry https://orcid.org/0000-0002-6081-0350

References

[1] Vozniy O V and Yeom G Y 2009 High-energy negative ion beam obtained from pulsed inductively coupled plasma for charge-free etching process *Appl. Phys. Lett.* **94** 1–4
[2] Donnelly V M and Kornblit A 2013 Plasma etching: yesterday, today and tomorrow *J. Vac. Sci. Technol.* A **31** 050825
[3] Rafalskyi D and Aanesland A 2016 Brief review on plasma propulsion with neutralizer-free systems *Plasma Sources Sci. Technol.* **25** 043001
[4] Lafleur T, Rafalskyi D and Aanesland A 2015 Alternate extraction and acceleration of positive and negative ions

from a gridded plasma source *Plasma Sources Sci. Technol.* **24** 015005
[5] Aanesland A, Rafalskyi D, Bredin J, Grondein P, Oudini N, Chabert P, Levko D, Garrigues L and Hagelaar G 2015 The PEGASES gridded ion-ion thruster performance and predictions *IEEE Trans. Plasma Sci.* **43** 321–6
[6] Ueno A, Oguri H, Ikegami K, Namekawa Y and Ohkoshi K 2010 Interesting experimental results in Japan proton accelerator research complex H- ion-source development (invited) *Rev. Sci. Instrum.* **81** 1–7
[7] Peters J 2000 Negative ion sources for high energy accelerators (invited) *Rev. Sci. Instrum.* **71** 1069–74
[8] Moehs D P, Peters J and Sherman J 2005 Negative hydrogen ion sources for accelerators *IEEE Trans. Plasma Sci.* **33** 1786–98
[9] Faircloth D and Lawrie S 2018 An overview of negative hydrogen ion sources for accelerators *New J. Phys.* **20** 025007
[10] Fantz U, Wünderlich D, Riedl R, Heinemann B and Bonomo F 2020 Achievement of the ITER NBI ion source parameters for hydrogen at the test facility ELISE and present Status for deuterium *Fusion Eng. Des.* **156** 111609
[11] Hemsworth R S *et al* 2017 Overview of the design of the ITER heating neutral beam injectors *New J. Phys.* **19** 025005
[12] Bacal M and Wada M 2015 Negative hydrogen ion production mechanisms *Appl. Phys. Rev.* **2** 021305
[13] Santoso J, Manoharan R, O'Byrne S and Corr C S 2015 Negative hydrogen ion production in a helicon plasma source *Phys. Plasmas* **22** 093513
[14] Hemsworth R *et al* 2009 Status of the ITER heating neutral beam system *Nucl. Fusion* **49** 045006
[15] Fantz U, Franzen P and Wünderlich D 2012 Development of negative hydrogen ion sources for fusion: experiments and modelling *Chem. Phys.* **398** 7–16
[16] Bacal M, McAdams R and Surrey E 2014 Extracted H^- ion current enhancement due to caesium seeding at different plasma grid bias *Rev. Sci. Instrum.* **85** 02B103
[17] Hemsworth R S and Boilson D 2019 *Research, Design and Development Needed to Realise a Neautral Beam Injection System for a Fusion Reactor* (Intech Open)
[18] Schiesko L, Carrère M, Cartry G and Layet J M 2008 H^- production on a graphite surface in a hydrogen plasma *Plasma Sources Sci. Technol.* **17** 035023
[19] Sasao M, Moussaoui R, Kogut D, Ellis J, Cartry G, Wada M, Tsumori K and Hosono H 2018 Negative-hydrogen-ion production from a nanoporous $12CaO.7Al_2O_3$ electride surface *Appl. Phys. Express* **11** 066201
[20] Cartry G *et al* 2017 Alternative solutions to caesium in negative-ion sources: a study of negative-ion surface production on diamond in H_2/D_2 plasmas *New J. Phys.* **19** 025010
[21] Smith G J, Ellis J, Moussaoui R, Pardanaud C, Martin C, Achard J, Issaoui R, Gans T, Dedrick J P and Cartry G 2020 Enhancing surface production of negative ions using nitrogen doped diamond in a deuterium plasma *J. Phys. D: Appl. Phys.* **53** 465204
[22] Smith G J, Tahri L, Achard J, Issaoui R, Gans T, Dedrick J P and Cartry G 2021 Surface production of negative ions from pulse-biased nitrogen doped diamond within a low-pressure deuterium plasma *J. Phys. D: Appl. Phys.* **54** 435201
[23] Kumar P, Ahmad A, Pardanaud C, Carrère M, Layet J M, Cartry G, Silva F, Gicquel A and Engeln R 2011 Enhanced negative ion yields on diamond surfaces at elevated temperatures *J. Phys. D: Appl. Phys.* **44** 372002
[24] Ahmad A, Pardanaud C, Carrère M, Layet J M, Gicquel A, Kumar P, Eon D, Jaoul C, Engeln R and Cartry G 2014 Negative-ion production on carbon materials in hydrogen plasma: influence of the carbon hybridization state and the hydrogen content on H^- yield *J. Phys. D: Appl. Phys.* **47** 085201
[25] Schiesko L, Carrère M, Layet J M and Cartry G 2010 A comparative study of H^- and D^- production on graphite surfaces in H_2 and D_2 plasmas *Plasma Sources Sci. Technol.* **19** 045016
[26] Kogut D, Moussaoui R, Ning N, Faure J B, Layet J M, Farley T, Achard J, Gicquel A and Cartry G 2019 Impact of positive ion energy on carbon-surface production of negative ions in deuterium plasmas *J. Phys. D: Appl. Phys.* **52** 1–26
[27] Cartry G, Schiesko L, Hopf C, Ahmad A, Carrère M, Layet J M, Kumar P and Engeln R 2012 Production of negative ions on graphite surface in H_2/D_2 plasmas: experiments and srim calculations *Phys. Plasmas* **19** 063503
[28] Kahn A 2015 Fermi level, work function and vacuum level *Mater. Horiz.* **3** 7–10
[29] Guichar G M, Garry G A and Sebenne C A 1979 Photoemission yield spectroscopy of electronic surface states on germanium (111) surfaces *Surf. Sci.* **85** 326–34
[30] Fowler R 1931 The analysis of photoelectric sensitivity curves for clean metals at various temperatures *Phys. Rev.* **38** 45
[31] Eastman D E 1970 Photoelectric work functions of transition, rare-earth and noble metals *Phys. Rev.* B **2** 1–2
[32] Rotermund H H, Jakubith S, Kubala S, von Oertzen A and Ertl G 1990 Investigation of surfaces by scanning photoemission microscopy *J. Electron Spectrosc. Relat. Phenom.* **52** 811–9
[33] Akbi M and Lefort A 1998 Work function measurements of contact materials for industrial use *J. Phys. D: Appl. Phys.* **31** 1301–8
[34] Wong K, Tikhonov G and Kresin V V 2002 Temperature-dependent work functions of free alkali-metal nanoparticles *Phys. Rev.* B **66** 1254011–5
[35] Prem A and Kresin V V 2012 Photoionization profiles of metal clusters and the Fowler formula *Phys. Rev.* A **85** 8–11
[36] Akbi M, Bouchou A and Zouache N 2014 Effects of vacuum heat treatment on the photoelectric work function and surface morphology of multilayered silver-metal electrical contacts *Appl. Surf. Sci.* **303** 131–9
[37] Gutser R, Wimmer C and Fantz U 2011 Work function measurements during plasma exposition at conditions relevant in negative ion sources for the ITER neutral beam injection *Rev. Sci. Instrum.* **82** 023506
[38] Cristofaro S, Friedl R and Fantz U 2020 Correlation of Cs flux and work function of a converter surface during long plasma exposure for negative ion sources in view of ITER *Plasma Res. Express* **2** 035009
[39] Friedl R 2016 Enhancing the accuracy of the Fowler method for monitoring non-constant work functions *Rev. Sci. Instrum.* **87** 043901
[40] Diederich L, Küttel O M, Ruffieux P, Pillo T, Aebi P and Schlapbach L 1998 Photoelectron emission from nitrogen- and boron-doped diamond (100) surfaces *Surf. Sci.* **417** 41–52
[41] Diederich L, Küttel O M, Aebi P and Schlapbach L 1998 Electron affinity and work function of differently oriented and doped diamond surfaces determined by photoelectron spectroscopy *Surf. Sci.* **418** 219–39
[42] Schiesko L, Carrère M, Layet J M and Cartry G 2009 Negative ion surface production through sputtering in hydrogen plasma *Appl. Phys. Lett.* **95** 19–22
[43] Smith G J 2021 Negative ion production in low temperature hydrogen plasmas *PhD Thesis* University of York
[44] Rafalskyi D, Dudin S and Aanesland A 2015 Magnetized retarding field energy analyzer measuring the particle flux

and ion energy distribution of both positive and negative ions *Rev. Sci. Instrum.* **86** 053302
[45] Taccogna F *et al* 2021 Latest experimental and theoretical advances in the production of negative ions in Caesium-free plasmas *Eur. Phys. J.* D **75** 227
[46] Achkasov K, Moussaoui R, Kogut D, Garabedian E, Layet J M, Simonin A, Gicquel A, Achard J, Boussadi A and Cartry G 2019 Pulsed DC bias for the study of negative-ion production on surfaces of insulating materials in low pressure hydrogen plasmas *J. Appl. Phys.* **125** 033303
[47] Jain S C 1952 The thermionic constants of metals and semi-conductors I. Graphite *Proc. R. Soc.* A **213** 143–57
[48] Lang N D and Nørskov J K 1983 The theory of ionization probability in sputtering *Phys. Scr.* **1983** 15–18
[49] Borisov A G and Esaulov V A 2000 Negative ion formation in the scattering of atoms and ions from dielectric surfaces *J. Phys.: Condens. Matter.* **12** R177–206
[50] Spicer W E 1993 Modern theory and applications of photocathodes *Proc. SPIE* **2022** 18–35
[51] Borisov A G, Sidis V and Winter H 1996 Diabatic energy level confluence: the mechanism of negative ion conversion of neutral atoms in grazing scattering from insulator surfaces *Phys. Rev. Lett.* **77** 1893–6
[52] Roncin P, Borisov A G, Khemliche H, Momeni A, Mertens A and Winter H 2002 Evidence for F^- formation by simultaneous double-electron capture during scattering of F^- from a LiF(001) surface *Phys. Rev. Lett.* **89** 2–5
[53] Borisov A G, Sidis V, Roncin P, Momeni A, Khemliche H, Mertens A and Winter H 2003 F^- formation via simultaneous two-electron capture during grazing scattering of F^+ ions from a LiF(001) surface *Phys. Rev.* B **67** 13
[54] Scheer J A, Wieser M, Wurz P, Bochsler P, Hertzberg E, Fuselier S A, Koeck F A, Nemanich R J and Schleberger M 2005 High negative ion yield from light molecule scattering *Nucl. Instrum. Methods Phys. Res.* B **230** 330–9